A&A 569, A6 (2014)
DOI: 10.1051/0004-6361/201423548

Astronomy & Astrophysics

Molecular tendrils feeding star formation in the Eye of the Medusa

The Medusa merger in high resolution ^{12}CO 2–1 maps

S. König[1], S. Aalto[2], L. Lindroos[2], S. Muller[2], J. S. Gallagher III[3], R. J. Beswick[4], G. Petitpas[5], and E. Jütte[6]

[1] Institut de Radioastronomie Millimétrique, 300 rue de la Piscine, Domaine Universitaire, 38406 Saint Martin d'Hères, France
e-mail: koenig@iram.fr
[2] Chalmers University of Technology, Department of Earth and Space Sciences, Onsala Space Observatory, 43992 Onsala, Sweden
[3] Department of Astronomy, University of Wisconsin, 475 N. Charter Street, Madison, WI 53706, USA
[4] University of Manchester, Jodrell Bank Centre for Astrophysics, Oxford Road, Manchester, M13 9PL, UK
[5] Harvard-Smithsonian Center for Astrophysics, 60 Garden Street, Cambridge, MA 02138, USA
[6] Astronomisches Institut Ruhr-Universität Bochum, Universitätsstraße 150, 44780 Bochum, Germany

Received 31 January 2014 / Accepted 23 June 2014

ABSTRACT

Studying molecular gas properties in merging galaxies gives us important clues to the onset and evolution of interaction-triggered starbursts. NGC 4194 (the Medusa merger) is particularly interesting to study, since its FIR-to-CO luminosity ratio rivals that of ultraluminous galaxies (ULIRGs), despite its lower luminosity compared to ULIRGs, which indicates a high star formation efficiency (SFE) that is relative to even most spirals and ULIRGs. We study the molecular medium at an angular resolution of $0.65'' \times 0.52''$ ($\sim 120 \times 98$ pc) through our observations of ^{12}CO 2–1 emission using the Submillimeter Array (SMA). We compare our ^{12}CO 2–1 maps with the optical *Hubble* Space Telescope and high angular resolution radio continuum images to study the relationship between molecular gas and the other components of the starburst region. The molecular gas is tracing the complicated dust lane structure of NGC 4194 with the brightest emission being located in an off-nuclear ring-like structure with ~320 pc radius, the Eye of the Medusa. The bulk CO emission of the ring is found south of the kinematical center of NGC 4194. The northern tip of the ring is associated with the galaxy nucleus, where the radio continuum has its peak. Large velocity widths associated with the radio nucleus support the notion of NGC 4194 hosting an active galactic nucleus. A prominent, secondary emission maximum in the radio continuum is located inside the molecular ring. This suggests that the morphology of the ring is partially influenced by massive supernova explosions. From the combined evidence, we propose that the Eye of the Medusa contains a shell of swept up material where we identify a number of giant molecular associations. We propose that the Eye may be the site of an efficient starburst of 5–7 $M_\odot\,\mathrm{yr}^{-1}$, but it would still constitute only a fraction of the 30–50 $M_\odot\,\mathrm{yr}^{-1}$ star formation rate of the Medusa. Furthermore, we find that ~50% of the molecular mass of NGC 4194 is found in extended filamentary-like structures tracing the minor and major axis dust lanes. We suggest that molecular gas is transported along these lanes, providing the central starburst region with fuel. Interestingly, a comparison with locations of super star clusters (SSCs) reveal that the molecular gas and the SSCs are not co-spatial.

Key words. galaxies: evolution – galaxies: individual: NGC 4194 – galaxies: starburst – galaxies: active – radio lines: ISM – ISM: molecules

1. Introduction

The focus on merger studies often lies on major-major (equal mass spirals) mergers and their evolution, although minor (unequal-mass) mergers constitute the major phase of interactions in the local Universe and at higher redshifts. Understanding how the gas is feeding starburst and active galactic nucleus (AGN) activities in these objects is therefore paramount in understanding the overall evolution of the Universe. In a numerical simulation study of minor- or intermediate mergers, Bournaud et al. (2005) found that the gas brought in by the disturbing companion galaxy is generally found at large radii in the merger remnant. The gas returns to the system from tidal tails and often forms rings – polar, inclined or equatorial – that will appear as dust lanes when seen edge-on (e.g., Combes 1988; Shlosman et al. 1989).

Evidence has been presented for an increased fraction of star formation happening in clusters within starbursts that are compared to that in quiescent galaxies, which potentially are linked to the interstellar medium (ISM) structure changes, while the starburst process takes place (Kennicutt & Evans 2012). Massive, young star clusters (super star clusters (SSCs), 10^5–10^8 $M_\odot$) are observed to form in on-going starbursts, such as those associated with interactions and (minor and major) mergers and those in smaller numbers in other types of galaxies with elevated star formation rates (SFR; e.g., Larsen 2002; de Grijs et al. 2003; Mora et al. 2009).

A nearby example of a surprisingly efficient starburst is the inner 2 kpc of the Medusa merger (NGC 4194). With a luminosity of $L_{\rm FIR} = 8.5 \times 10^{10}$ $L_\odot$ (at D = 39 Mpc, $1'' = 189$ pc), this E+S minor merger is an order of magnitude fainter than well known ultraluminous galaxies (ULIRGs), such as Arp 220 (Aalto & Hüttemeister 2000; Manthey et al. 2008). Despite the moderate FIR luminosity, NGC 4194 has a $L_{\rm FIR}/L_{\rm CO}$ ratio similar to those typical for ULIRGs, which suggests that its star formation efficiency (SFE) rivals that of the compact ULIRGs. Despite this, its CO/HCN 1–0 luminosity ratio is ~25, indicating that the fraction of dense gas is significantly lower despite the similar SFE to ULIRGs. The picture becomes even more interesting when one considers that most of the ongoing star formation in

NGC 4194 is not traced by the FIR or radio emission: The Hα SFR is ~40 $M_\odot\,\mathrm{yr}^{-1}$ (Hancock et al. 2006), while the FIR estimated SFR is 6–7 $M_\odot\,\mathrm{yr}^{-1}$. The spatial correlation between the molecular gas distribution and the 1.4 GHz continuum is also poor (unlike the case for most nearby galaxies, Aalto & Hüttemeister 2000). In NGC 4194, a large fraction of the star formation is going on in SSCs with a kpc-scale distribution, which is separated from the molecular gas distribution. No obvious correlation between these young SSCs (5–15 Myr) and the CO can be found. The CO emission also traces the two prominent dust lanes that cross the central region and extends into the northern tidal tail. The majority of the CO (~70%, ^{12}CO, Aalto et al. 2001; Lindroos 2011) is found in the central 2 kpc of the galaxy with 15% of this gas (^{13}CO, Aalto et al. 2010), which resides in a compact region 1.5″ south of the radio nucleus. The knots where the optically traced star formation is going on only occasionally correlate with the radio continuum or the molecular distribution.

Throughout the paper, we are concerned with pure rotational transitions in CO between upper state $J' = 2$ and lower state $J'' = 1$ that are labeled 2–1.

In this paper, we present a study of the molecular gas close to the AGN in the Medusa merger. In Sect. 2, we describe the observations and data reduction; Sect. 3 reports on the results of the observations. The discussion follows in Sects. 4 and 5, and conclusions are drawn in Sect. 6.

2. Observations

NGC 4194 was observed with the SubMillimeter Array (SMA) on February 21, 2010 in the very-extended configuration and on April 8 in the compact configuration, which provides the highest angular resolution CO observations of NGC 4194 to date. For analysis purposes, we shifted the phase center to the position of the 1.4 GHz radio continuum peak at α = 12:14:09.660 and δ = +54:31:35.85 (J2000, Beswick et al. 2005). The heterodyne receivers were tuned to the redshifted frequency of the ^{12}CO 2–1 transition at 228.63 GHz in the upper sideband, while the ^{13}CO 2–1 transition was observed in the lower sideband. With baseline lengths between 38 m and 509 m, these SMA imaging data are sensitive to scales smaller than 16.5″. The correlator was configured to provide a spectral resolution of 0.8125 MHz (corresponding to a velocity resolution of ~1.1 km s^{-1}). The bright quasars J0854+201 and 3C 454.3 were used as bandpass calibrators; Vesta and Ganymede were observed as primary flux calibrators, and we regularly observed the close-by quasars J1153+72, J0927+390, and J0721+713 for complex gain calibration.

After calibration within the dedicated MIR/IDL SMA reduction package, both visibility sets were converted into FITS format and imported in the GILDAS/MAPPING[1] and AIPS packages for further imaging.

For the ^{12}CO 2–1 data, sets of visibilities from the compact and very extended configuration observations were combined and deconvolved using the Clark method (Clark 1980) with robust weighting. This results in a synthesized beam size of 0.65″ × 0.52″ with a position angle (PA) of 67°. We smoothed the data to a velocity resolution of ~25 km s^{-1}, which yields a 1σ rms noise level per channel of ~6.8 mJy beam^{-1}. To look at the most compact component in the CO distribution, we used robust weighting, putting additional weight on the longest baselines, resulting in a 0.43″ × 0.38″ beam with a position angle of 52°. This provides a very high resolution map in which we look for giant molecular associations (GMAs).

To compare our results with high resolution images of the radio continuum structure of NGC 4194, we obtained 1.4 GHz radio continuum data at the VLA (Jütte et al., in prep.) and combined them with published data from Beswick et al. (2005). These combined data have an angular resolution of 0.50″ × 0.52″ corresponding to a linear scale of ~95 pc × 98 pc.

3. Results

3.1. ^{12}CO 2–1

3.1.1. Integrated intensity

The integrated intensity map (Fig. 1a) shows an asymmetric CO 2–1 distribution in the east-west direction. The eastern part contains the peak of the CO emission at about 1–1.5″ southeast of the radio continuum peak, which is located in the northern part of a ring-like structure or possibly tightly wound spiral arms, with a maximum extent of ~4″ that has no CO emission peak at its center (Fig. 1a).

The total CO 2–1 flux within the 2σ contours (see Fig. 1a) amounts to 411.0 ± 4.1 Jy km s^{-1}. A comparison of the total CO 2–1 flux within the inner 13″ of NGC 4194 obtained from single-dish observations Casoli et al. (1992) shows that we recover approximately 50% (~642 Jy km s^{-1}) of the flux with our SMA observations. Our high-resolution data are sensitive to structures smaller than 16.5″ (see Sect. 2), hence 50% of the flux seems to be associated with structures larger than this size. Approximately one third of the total flux is located in the east of the ring-like structure (128.3 ± 4.5 Jy km s^{-1}) and one fourth (S_ν = 103.7 ± 2.7 Jy km s^{-1}) in the elongated western part of the CO 2–1 distribution.

Casoli et al. (1992) show the integrated intensity of CO 2–1 to be 80% of that of CO 1–0. Thus, we can scale our CO 2–1 flux by this amount to obtain an estimated CO 1–0 flux for our observations. Assuming a CO-to-H_2 conversion factor of $X_{\mathrm{CO}} = 2.0 \times 10^{20}$ cm^{-2} (K km s^{-1})$^{-1}$ (Narayanan et al. 2012; Sandstrom et al. 2013)[2], this then translates to a mass of ~1.6×10^9 $M_\odot$ for the overall CO 2–1 molecular gas distribution. The molecular gas in the ring sums up to a mass of ~4.1×10^8 $M_\odot$.

3.1.2. Kinematics of the ^{12}CO 2–1 gas

Figures 1c, d, and 2 show the velocity field and the velocity dispersion of the CO 2–1 emission in NGC 4194. *The velocity fields* (Figs. 1c, d) show a rather regular pattern for the main body of the molecular emission, which is typical for solid body rotation, with a position angle of −20° in which the velocities range from 2400 km s^{-1} to 2700 km s^{-1}. The contours of the velocity field in the western component of the molecular gas emission, which we call the western arm, deviate from the typical solid-body rotation pattern. These deviations could be indicators for streaming motions, as found in other galaxies, such as in M 51 and NGC 5248 (Aalto et al. 1999; van der Laan et al. 2013). Aalto & Hüttemeister (2000) have shown that molecular gas is associated with the dust lanes that cross NGC 4194 in front of the main body. The velocities of this gas emission are almost constant across large distances along the way to the center. This

[1] http://www.iram.fr/IRAMFR/GILDAS

[2] We will study the influence of the distribution of molecular gas on X_{CO} through different molecular transitions in paper II (König et al., in prep.).

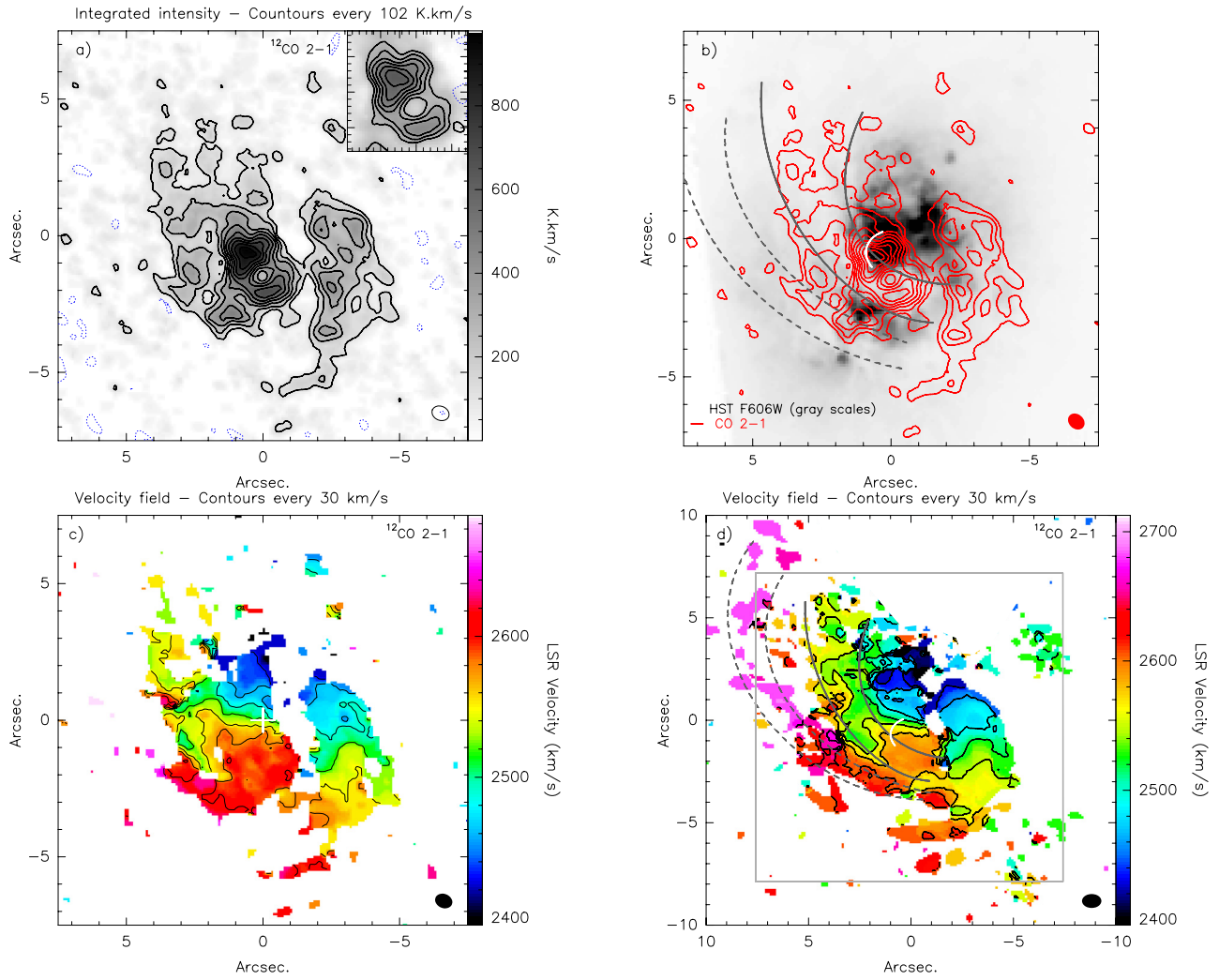

Fig. 1. Integrated intensity map (*upper left*) and velocity field (*bottom left*) of the high resolution CO 2−1 emission (0.65″ × 0.52″), velocity field of the low resolution CO 2−1 emission (*bottom right*, 0.95″ × 0.68″) in NGC 4194, and an overlay of the high resolution ^{12}CO 2−1 emission contours on top of an HST WFPC2 *F606W* filter image (*top right*). The noise level in the integrated intensity map is 1.3 Jy km s^{-1}. Contours for the integrated intensity map start at 2σ in steps of 2σ; the first negative contour at −2σ is shown as a dotted contour. The velocity range plotted in the velocity field is between 2400 km s^{-1} and 2700 km s^{-1}; contours range from 2400 km s^{-1} to 2640 km s^{-1}. The gray, gray-dashed, and white curves in the HST overlay and lower-resolution velocity field represent the locations of the most important dust lanes. The solid line box in the lower-resolution velocity field represents the field-of-view shown in the higher-resolution velocity field. North is up, east to the left. The position of the 1.4 GHz continuum peak is marked by a white cross (Beswick et al. 2005).

behavior changes just before the gaseous material turns into the plane of the merger (see, e.g., the most eastern CO associated with the eastern dust lane, as seen in Fig. 1c). This seems to be true as well for the dust lane located further west and closer to the center of NGC 4194.

The velocity dispersion distribution in the Medusa (Fig. 2a) shows the most prominent peak at the position of the radio continuum peak (Beswick et al. 2005) with a line dispersion roughly twice the size than in the rest of the CO distribution. The line dispersion at this peak rises to about 70 km s^{-1} compared to the surrounding material where the dispersion lies between 15 km s^{-1} and 35−40 km s^{-1}.

The position-velocity diagrams along the major (north to south, left panel) and the minor (east to west, right panel) axes are shown in Fig. 3. Both pv diagrams were obtained by averaging over slits with a width of 1″ with one positioned along the axis of solid-body rotation and the other perpendicular to that direction. Both slits do include emission from parts of the molecular ring-like structure. In the major axis pv diagram (Fig. 3a), the pattern of the rather smooth solid-body rotation, especially when considering the merger history, already seen in the velocity field (Figs. 1c, d) has been reproduced. The two most distinctive peaks in this distribution represent the structure of the ring-like gas component at the center of NGC 4194. The minor axis pv diagram (Fig. 3b) shows two distinct components in the distribution: one molecular emission peak with a steep velocity gradient across a few arcseconds in the west and two distribution peaks close to the nucleus. The feature with the steep velocity gradient originates from gas in the same location that already showed an exceptional behavior in the velocity field (Figs. 1c, d) in the western arm. This might hint toward the presence of streaming motions in the western arm. The second component close to the nucleus represents the gas in the ring-like structure by showing a difference in velocity for the different locations in this structure.

The rotation curve: we fitted a Brandt curve (Eq. (1), Brandt 1960) to the velocity field of the molecular emission using a fixed inclination value of 40° (from the optical isophotes, Aalto & Hüttemeister 2000). The result is shown in Fig. 3a with the

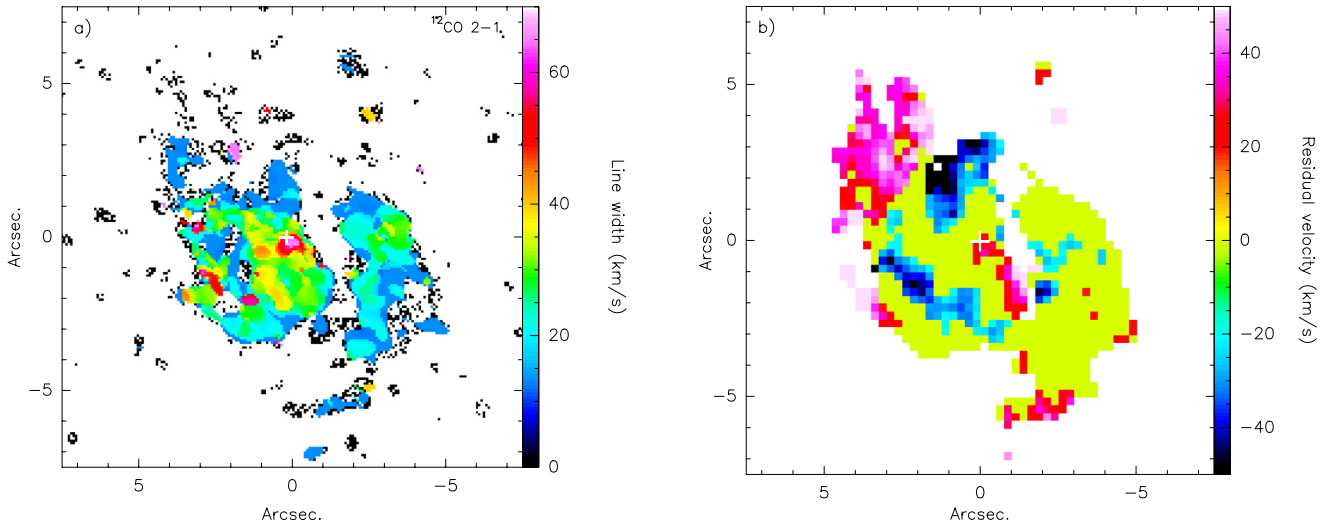

Fig. 2. Velocity dispersion map of the high-resolution CO 2−1 emission (*left*). Map showing the residuals in the velocity field after the subtraction of the rotation curve from the CO velocity field (*right*). Residuals in the range ±20 km s^{-1}, which corresponds to the noise limit in the residuals map, are plotted in light green; regions with values larger than that are depicted in red (positive values) and blue (negative values). The white crosses mark the peak position of the radio continuum from Beswick et al. (2005).

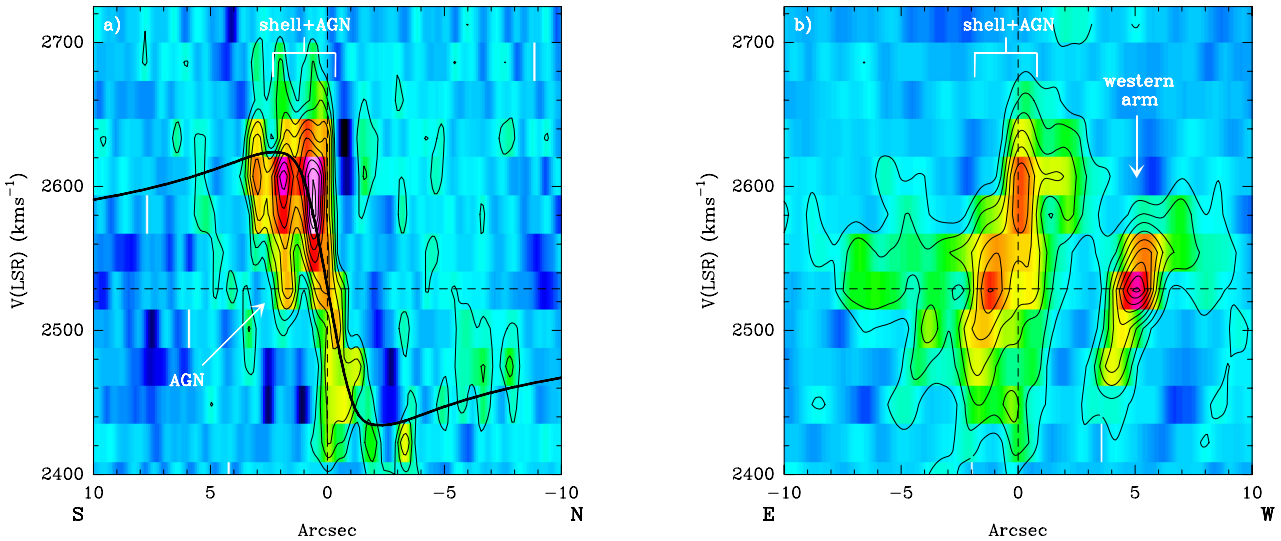

Fig. 3. CO 2−1 position-velocity diagrams along the major (north-south, *left*) and the minor (east-west, *right*) axes of the NGC 4194 obtained from the high-resolution data cube within a slit width of 1″. The contour levels start at 1.5σ in steps of 1.5σ. The colors range from 0 to 0.1 mJy/beam. The result of the fitted Brandt rotation curve, using a fixed inclination value of 40°, is shown on *the left*.

pv diagrams for the major and minor axes. The fitted rotation curve starts to flatten (fall) at a radius $R_{\rm max}$ of 2.3″, which indicates a deprojected rotational velocity $v_{\rm rot}$ of 148 km s^{-1}. The dynamical mass inferred from these values is $M_{\rm dyn} \sim 2.2 \times 10^9\ M_\odot$. A plot of the residuals after subtracting the fit from the velocity field is presented in Fig. 2b. There, the residuals in the western arm again illustrate the presence of typical features of streaming motions in this location. We cannot draw clear conclusions whether or not some type of streaming motion is also going on in the eastern part of the molecular emission as well due to the likely overlap of different structures and processes taking place there.

$$v_{\rm rot}\,(R) = \frac{v_{\rm max}\,(R/R_{\rm max})}{\left[\frac{1}{3} + \frac{2}{3}\,(R/R_{\rm max})^{\rm n}\right]^{\frac{3}{2n}}}. \quad (1)$$

3.2. The Eye of the Medusa

Figures 1a and b show a top-heavy ring-like structure, where the majority of the molecular mass is located in the northern part of the structure. This structure dominates the CO 2−1 emission in the eastern part of NGC 4194, which is close to its center. We determined the ring-like structure to have a molecular mass of ~$4.1 \times 10^8\ M_\odot$ (corresponding to one third of the total CO 2−1 mass in these data), enclosed in a radius of ~1.7″ (equivalent to ~320 pc) with a width of 1.5″ (~285 pc) in the northern part of the ring and a width of 0.9″ (~170 pc) in the south. The nucleus of NGC 4194 is located at the northern tip of the ring, while the bulk emission of the ring is located south of the kinematical center in a molecular shell or bubble. In contrast to 1.4 GHz radio continuum observations (Fig. 6, Beswick et al. 2005), where a secondary peak is located at the center of the ring, the CO 2−1 does not show a clear emission peak at its center. This structure was named the Eye of the Medusa (Lindroos 2011).

Table 1. Properties of the identified GMA candidates.

GMA	RA(2000)	Dec(2000)	Spherical radius[a]	v_0[b]	Dispersion[c]	Mass
	[h] [m] [s]	[°] [′] [″]	[pc]	[km s^{-1}]	[km s^{-1}]	[$M_\odot$]
GMA 1	12:14:09.805	54:31:35.54	83	2585	42	1.0×10^7
GMA 2	12:14:09.749	54:31:36.01	103	2501	52	1.5×10^7
GMA 3	12:14:09.631	54:31:36.08	92	2467	44	1.2×10^7
GMA 4	12:14:09.737	54:31:35.47	132	2557	57	3.4×10^7
GMA 5	12:14:09.674	54:31:35.76	114	2508	67	2.8×10^7
GMA 6	12:14:09.632	54:31:35.44	92	2510	62	1.6×10^7
GMA 7	12:14:09.749	54:31:34.72	123	2595	40	3.1×10^7
GMA 8	12:14:09.667	54:31:35.13	130	2595	45	3.5×10^7
GMA 9	12:14:09.612	54:31:33.90	103	2599	45	1.9×10^7
GMA 10	12:14:09.577	54:31:34.21	130	2575	59	3.1×10^7
GMA 11	12:14:09.547	54:31:34.55	92	2588	47	1.3×10^7

Notes. [(a)] The source size was determined by fitting a Gaussian to the position of the respective GMA in the uv table. The values given here are the FWHM of the fitted Gaussian deconvolved from the synthesized beam. The typical (average) error for the fit to the GMA size is about 20%. [(b)] Typical errors are on the order of 5−10 km s^{-1}. [(c)] Typical errors are on the order of 10%.

The CO 2−1 emission distribution of the Eye, shows hot spots of enhanced ^{12}CO 2−1 intensity (Fig. 5). The mass estimates of some of those clumps place them in the mass range for GMAs (Table 1, Vogel et al. 1988). We identified GMA candidates as peaks (peak values larger than three times the noise level) in the integrated CO 2−1 map and with a clear detection ($\gtrsim5\sigma$) in the spectrum. The spectra were obtained by averaging over an area of 5×5 pixels around the peak. This resulted in the identification of 11 GMA candidates. How many of these candidates are real is an issue that can only be solved by higher resolution, high-sensitivity observations. The molecular properties of the Eye are discussed in Sect. 4.

4. Molecular structure of NGC 4194

Two major dust lanes to the east of the nucleus, which are visible in the optical (e.g., HST, Fig. 1b), cross the main optical body of NGC 4194. The one crossing directly below the galaxy's dynamical center is associated with large parts of the molecular gas. The second dust lane further to the east crosses further south of the nucleus. The molecular gas is clearly associated with both dust lanes tracing filamentary-like features (see the lower resolution velocity field in Fig. 1d). The CO emission in the northeast stretching out toward these dust lanes appears filamentary. The western part of the CO distribution with a north-south orientation agrees well with peaks c and d found by Aalto & Hüttemeister (2000) in their CO 1−0 data (see Fig. 7). There seems to be a gap in the CO distribution between the molecular gas in the east and the west, apart from a small connection between the two parts with a width of ∼1″. Within the asymmetric CO 2−1 emission distribution, the ring-like structure, the Eye of the Medusa, shows hot spots of enhanced ^{12}CO 2−1 intensity (Fig. 5). A more detailed discussion of these features can be found in Sect. 4.2.

Connected to the CO in the Eye seems to be a gas component that shows the highest velocity dispersion at the 1.4 GHz radio continuum peak found by Beswick et al. (2005). A weak AGN component might be present at this position in the center of NGC 4194. This is discussed in more detail in Sect. 4.1.

Observations of different star formation tracers have been reported covering the larger scale structures associated with the CO 1−0 observations and the dust lanes down to the region surrounding the nucleus of NGC 4194. Weistrop et al. (2004) and Hancock et al. (2006) found a number of stellar clusters in the UV and visible light (VIS, see, e.g., Figs. 8, 9). The majority of these clusters does not seem to be closely associated with the molecular gas. Indeed, most of these clusters are positioned in a void of molecular gas between the eastern and western parts in the CO 2−1 emission. For further details, see Sect. 4.3.

In Sect. 5.1, we compare the properties of NGC 4194 to other minor mergers and, in Sect. 5.2, we compare our results for NGC 4194 with galaxies that harbor molecular shells and blowouts.

4.1. The AGN

Several indicators speak in favor of the presence of an AGN in NGC 4194, even if it might be weak. X-ray and [Ne V] 14.3 μm line observations have shown the possibility for the presence of a small AGN contribution to the energy output of NGC 4194. Kaaret & Alonso-Herrero (2008) and Lehmer et al. (2010) suggest the presence of an AGN in the nucleus based on their 2−10 and 2−8 keV point source identifications and nuclear count rates. *Spitzer* observations of the [Ne V] 14.3 μm line yielded detections for Bernard-Salas et al. (2009) and Lehmer et al. (2010) which leads them to conclude the presence of a weak AGN being located in NGC 4194.

Spectra taken of the Eye from the high resolution data ($0.43''\times0.38''$) show a double-peaked velocity distribution (Fig. 4) with velocity components centered at ∼2600 km s^{-1} and at ∼2450 km s^{-1}. The latter component is only present in the region closest to the AGN (GMAs 3, 5 and 6). The gas mass determined from this velocity component is $\sim4.4\times10^7$ $M_\odot$. Isolating this velocity component and making an integrated intensity map confirms that this gas is only present in the northern part of the central high density gas complex (Fig. 5b). The total gas mass surrounding the AGN (both CO velocity components) results to $\sim1.1\times10^8$ $M_\odot$. The dynamical mass enclosed in this region is $\sim5.0\times10^8$ $M_\odot$. With their HI absorption observations, Beswick et al. (2005) were able to put a limit on the dynamical mass of the central nuclear region of $\sim2\times10^9$ $M_\odot$, which is in good agreement with the results from this work. This CO 2−1 complex is located at the unresolved center of the larger scale molecular gas reservoir in NGC 4194 (CO 1−0, see Fig. 7, Aalto & Hüttemeister 2000).

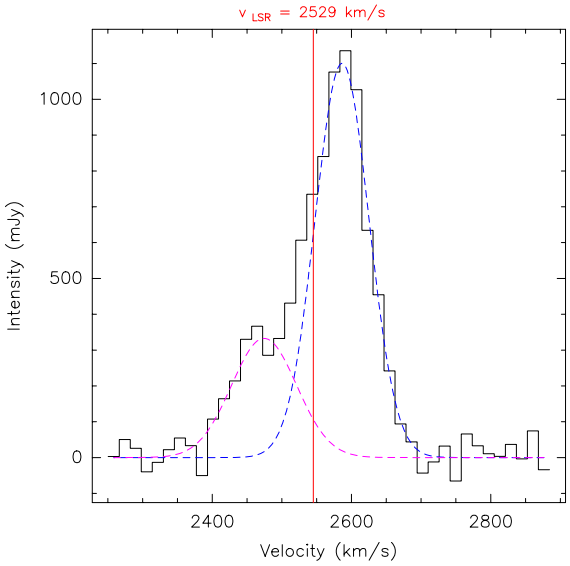

Fig. 4. Spectrum of the central high density gas region (Eye of the Medusa) containing the AGN and the shell. A Gaussian fit shows that the spectrum is well reproduced by two velocity components (magenta and blue). The velocity resolution is ~15 km s^{-1}. A closer view at the spectra at different positions in the central region shows that the gas represented by the velocity component centered at 2450 km s^{-1} (magenta) is only present close to the nucleus of NGC 4194.

Speaking against the presence of an AGN, however, are the findings from Beck et al. (2014). Their radio continuum and [Ne II] observations indicate the compact radio emission sources in NGC 4194 to be dense stellar clusters.

4.2. The structure of the Eye

The highest surface brightness CO 2−1 emission emerges in a ring-like structure south of the nucleus (Fig. 5b) – the Eye of the Medusa. The molecular gas in this complex seems to be connected to the 1.4 GHz radio continuum peak, which possibly marks the position of a weak AGN. Most of the gas, however, is associated with the eastern dust lane that comes in closest to the galactic center (Fig. 1). The center of the Eye is not located at the dynamical center of NGC 4194, as determined from the rotation curve (see Sect. 3.1.2). The location of the possible AGN in the northwestern part of this structure agrees with the center coordinates. This implies that this structure might not have been formed from purely dynamical processes (e.g., orbit crowding, resonances).

In Figs. 5 and 6 we show that there is a hole in the CO emission. Located right at the center of that hole is a secondary 1.4 GHz radio continuum peak (Fig. 6, see also Beswick et al. 2005). The radio continuum very nicely traces the peak of the gas in the northern part of the Eye but it seems to avoid gas in the southern part: the radio continuum peaks at the center of the structure where there is no CO, but most of the southern part of the CO in this region is not traced by the 1.4 GHz emission as is GMA 7 in the north. The radio continuum associated with GMA 8 most likely spills over from the peak at the AGN position.

The fact that the CO depression in the south of the ring-like structure corresponds to a secondary peak in the 1.4 GHz emission and the maximum in HI absorption against the continuum (Beswick et al. 2005), suggests that the hole in the CO 2−1 distribution might be a shell or bubble in the molecular gas caused by a massive explosion of supernovae (SNe). The funneling of the gas to the very center of NGC 4194 leeds to a burst of star formation in the central molecular gas. Subsequently, supernovae explode and the energy freed by the SNe going off drove the molecular gas outwards, which is away from the center of the explosion, thereby shaping the central molecular gas reservoir to the observed morphology: the expansion of the shell/bubble causes a spherical gas pile-up at the shock fronts, where new star formation is triggered and pinpoints the interaction between the accelerated shell/bubble material and the surrounding ISM. The result is the Eye of the Medusa, the molecular ring-like structure with a shell or bubble that we observe in the CO 2−1 emission.

$$E_0 = 5.3 \times 10^{-7} n_0^{1.12} v_{\rm sh}^{1.4} R^{3.12}. \quad (2)$$

To derive the energy output necessary for the formation of the shell/bubble with the properties we observe in our CO 2−1 data, we applied Chevalier's equation (Eq. (2), Chevalier 1974). Using a hydrogen number density of the surrounding pre-bubble medium of ~59 cm^{-3} (value determined from the density and volume of the surrounding gas not yet influenced by the expansion of the shell), a radius of 180 pc (the inner radial expansion of the shell material), and an expansion velocity of 55 km s^{-1} (from the pv diagram), we derive an energy output of 1.4×10^{55} ergs, which is the equivalent of ~10 000 SNe of type II. We derived the kinematical age, using $t_{\rm kin} \approx \alpha R/v$ where R is the radius of the shell or bubble, v is the expansion velocity, and α is a parameter to account for nonlinear expansion. We assume α to be ~0.5, a value in the middle of the range of possible values (Sakamoto et al. 2006). Due to the uncertainty in the assumption of α, we expect an uncertainty in the time estimate of a factor of 2. Hence, the kinematical age for the shell in NGC 4194 is $\sim 1.6 \times 10^6$ yr, and the supernova rate thus amounts to $\sim 6 \times 10^{-3}$ SN yr^{-1}. A comparison to other galaxies hosting shells/bubbles is discussed in Sect. 5.2.

Our data mapped at the highest resolution (beam: 0.43″ × 0.38″, PA = 52°, 1″ = 189 pc) revealed a clumpy structure in the Eye component of the CO 2−1 distribution, as in NGC 1097, NGC 1365, or NGC 1614, for example. We identified 11 possible GMAs (see Fig. 5); the majority (GMA 1 to GMA 8) are located in the northern part of the structure. Masses $M(H_2)$ between $\sim 1.0 \times 10^7$ $M_\odot$ and $\sim 3.6 \times 10^7$ $M_\odot$ place them in the mass range typically found for GMAs (Vogel et al. 1988). Their dispersion values and sizes (spherical radii) range from ~40 km s^{-1} to ~67 km s^{-1} and 35 pc to 56 pc, respectively. Due to their large velocity dispersion, the GMA candidates do not fall on the Larson size-linewidth law for molecular clouds (e.g., Larson 1981; Solomon et al. 1987) but instead lie above this relation. A comparison of the CO spectra of the GMA candidates reveals a single spectral peak in all GMAs not associated with gas surrounding the AGN position. The spectra of some of the GMAs in the northern part of the shell show a double-peaked emission line (GMA 5, 8) and broad line widths probably due to blending of the two velocity components (GMA 6). These three complexes are closest to the nucleus of NGC 4194. The GMAs 7 and 8 are located in the northern part of the shell; GMA 9 to 11 are located in the southern part. The majority of these hot spots of enhanced ^{12}CO 2−1 intensity (GMA 1, 4, 7, 9−11) is actually associated with the eastern dust lane that crosses the molecular gas shell. This can also be seen in NGC 1614, for example, where half of the GMAs identified in CO 2−1 observations are associated with dust lanes.

The average mass of the GMA candidates in NGC 4194 is $\sim 2.2 \times 10^7$ $M_\odot$, the line widths average at a value of ~120 km s^{-1}, and the fitted average FWHM size (spherical radius) of the GMAs is ~109 pc. The GMAs in NGC 1614 seem

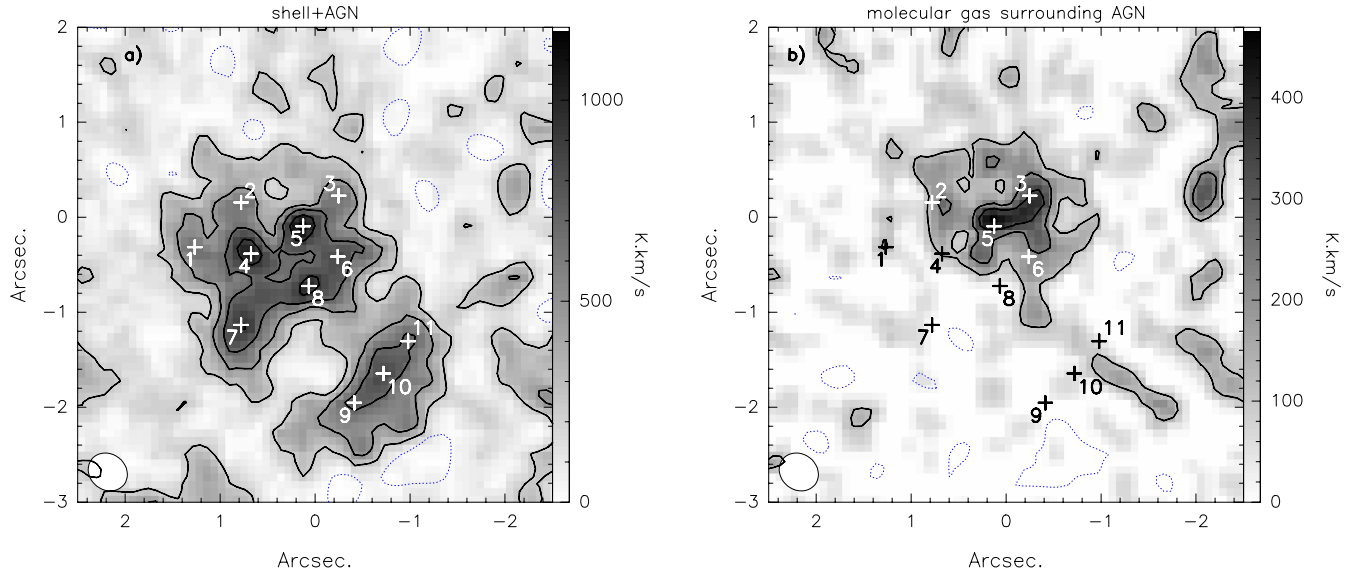

Fig. 5. Distribution of the central CO 2−1 emission in high resolution (*left*) and intensity distribution of the gas surrounding the AGN, which is associated only with the second velocity component in the CO 2−1 spectrum (*right*). Crosses and numbers from 1 to 11 mark the positions of the GMAs. GMA 5 is located at the peak position of the 1.4 GHz radio continuum (Beswick et al. 2005). The beam (0.43″ × 0.38″) is shown in the lower left corner of the panels. The contours are at every 1.0 Jy km s^{-1} starting at 1.0 Jy km s^{-1}; blue dotted contours are the negative counterparts of the lowest positive contour.

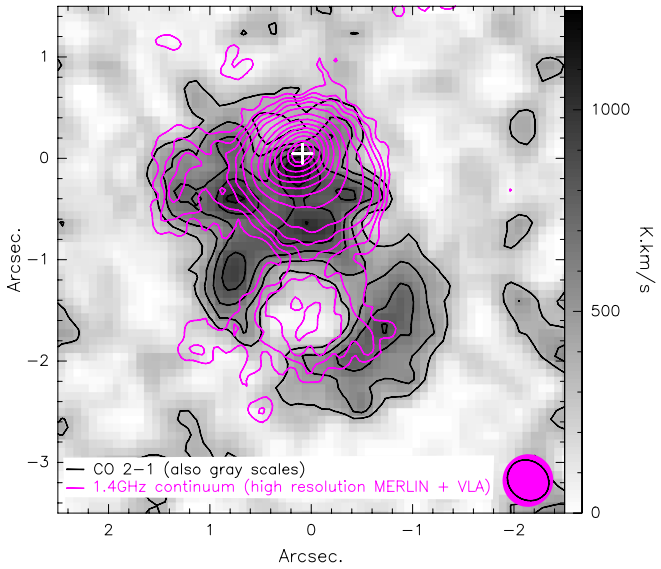

Fig. 6. Comparison of the high-resolution CO 2−1 emission with the high-resolution 1.4 GHz emission in the central region of the Medusa. Black contours and gray scale background represent the higher resolution CO 2−1 emission (0.43″ × 0.38″). The high-resolution combined MERLIN and VLA data are represented by magenta contours. The cross marks the position of the 1.4 GHz radio continuum peak of the MERLIN observations by Beswick et al. (2005). The beam sizes are depicted, according to the color schemes, in the lower right corner.

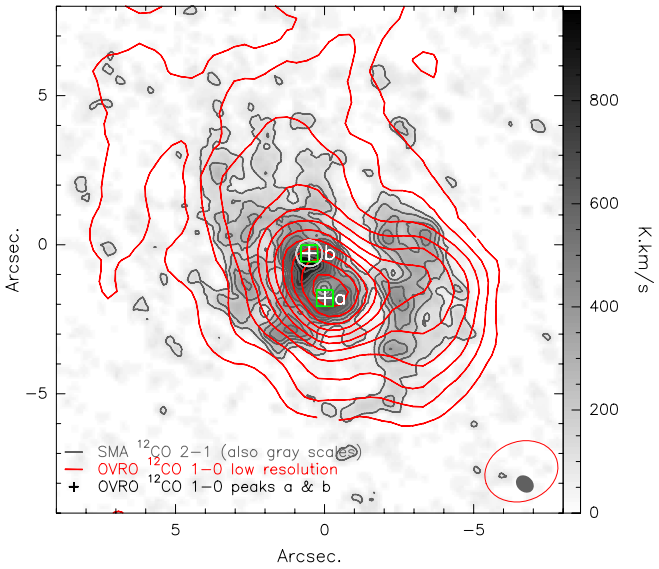

Fig. 7. Comparison of the SMA ^{12}CO 2−1 emission (gray scales) with OVRO ^{12}CO 1−0 low resolution data (Aalto & Hüttemeister 2000). The beam sizes are indicated in the lower right corner. White crosses mark the positions of peaks "a" and "b" found by Aalto & Hüttemeister (2000) in their high resolution data, squares represent the CO peaks located in the dust lane and the circle marks the peak position with a counterpart in Hα (Armus et al. 1990).

to lie on a different scale. They are on average more massive (6.0×10^7 $M_\odot$), show the same line widths (120 km s^{-1}), and are significantly larger in size (270 pc) than the GMAs in NGC 4194 (König et al. 2013). The size estimate is difficult, though. Therefore, this comparison criterion should not be overestimated. Another point to keep in mind is that the ring-structure in NGC 4194 is only half of the size of the ring in NGC 1614. Another galaxy bearing GMAs that are comparable to the ones in NGC 1614 is NGC 1097 (average size ∼250 pc, mass 9.2×10^7 $M_\odot$, line width 84 km s^{-1}, Hsieh et al. 2011), whereas the GMAs in NGC 1365 (line widths between 60 and 90 km s^{-1}, masses of $\sim 10^6$ $M_\odot$, Sakamoto et al. 2007) seem to be even less massive and have smaller line widths than the ones in NGC 4194.

4.3. Circumnuclear molecular gas and star formation

A number of different gas tracers has been observed toward NGC 4194 with different spatial resolutions. The CO 1−0, radio continuum (at 3.5 cm, 6 cm and 20 cm), and HST observations

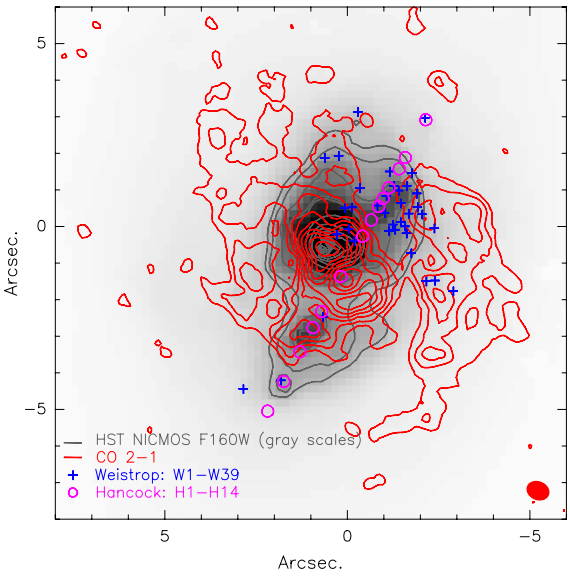

Fig. 8. Overlay of the ^{12}CO 2−1 emission contours on top of an HST WFPC2 *F606W* filter image. North is up, east to the left. Blue crosses indicate the positions of the star clusters that were found by Weistrop et al. (2004) in the UV; magenta circles represent the star clusters identified in the visible (Hancock et al. 2006). The CO beam size is indicated in the lower right corner.

(e.g., at wavelengths of 150 nm and 600 nm), for example, show brightness distribution peaks at the location of the AGN (e.g., Aalto & Hüttemeister 2000; Condon et al. 1990; Beswick et al. 2005; Armus et al. 1990; Weistrop et al. 2004). Spectroscopic Hα observations find the majority of the star formation going on in the central 8″ (Weistrop et al. 2012). Several star forming clusters have been identified in the UV (160 nm and 200 nm, Weistrop et al. 2004) and the VIS (430 nm and 780 nm, Hancock et al. 2006); some of them are associated with the AGN at the nucleus of NGC 4194 (Fig. 8).

Most of the brightness peaks identified in the high resolution CO 1−0 data (Aalto & Hüttemeister 2000) are situated in the main dust lane (peaks a, b, d, and e). Peaks a and b represent positions in the southern and northern part of the central high surface brightness density complex in the CO 2−1 maps; peaks c and d are located in the northern and the southern part of the western arm. Two of the CO 1−0 peaks (b and c) seem to be counterparts to brightness maxima found in Hα observations (see Fig. 7, Armus et al. 1990). Peak b is furthermore associated with the peak position in the high-resolution 1.4 GHz continuum maps (see, e.g., Fig. 6, Beswick et al. 2005).

Our CO 2−1 observations together with all these tracers indicate that a big part of the overall star forming activity seems to be on-going in the central few arcseconds around the AGN. However, to gain more insight into the locations and the properties of the star forming regions in the center of NGC 4194, further observations are needed. For example, high resolution Brγ narrow-band images would give valuable insight into the positions of regions of massive star formation; HCN/HCO$^+$ observations would help to distinguish high density regions ($n \gtrsim 10^4$ cm^{-3}).

The search for star clusters has yielded detections in the visible and in the UV wavelength regimes (see Figs. 8 and 9). Weistrop et al. (2004) used HST imaging to look for star clusters in the UV. They identified 39 young stellar clusters between the ages of 5 and 15 Myr distributed over the optical body of NGC 4194. Hancock et al. (2006) extended the properties of star clusters in this galaxy by identifying 14 clusters in a slit positioned along a position angle of 147° using visible and UV light. Some of the clusters from the two samples seem to coincide within the placement of the slit, but there are also clusters at slit positions in the visible light that seem to have no UV counterparts. The majority of the UV and VIS identified star clusters does not seem to be closely associated with the molecular gas. Indeed, most of these clusters are positioned in a void of molecular gas between the eastern and western parts in the CO 2−1 emission. Most of the UV-identified clusters are located in the north and west of the CO 2−1 distribution; none are associated with molecular gas in the east and north-east of the nucleus (Figs. 8, 9).

A comparison to the high resolution CO 2−1 shows that the GMAs closest to the nucleus (GMA 3, 5 and 6) seem to be associated with some of the Weistrop et al. (2004) UV clusters (Fig. 9). One of the clusters identified by Hancock et al. (2006) is also located in that region. The southern part of the CO shell, on the other hand, harbors no star clusters, although we identified three GMAs in that region. One of the VIS-identified star clusters, however, is located right at the center of the shell, where there is no CO, but the radio continuum has a secondary peak in this location.

Using the CO 2−1 data, we are now able to better distinguish between the higher density gas close to the nucleus and the lower density gas in the surrounding environment described by the CO 1−0 observations of Aalto & Hüttemeister (2000). Indeed, we find that the gas in the Eye closest to the nucleus is of higher surface brightness density than the larger scale CO emission. This reservoir of high-surface-brightness gas is located inside the solid body part of the rotation (Fig. 3). The gas surface density close to the nucleus amounts to $\sim 4.1 \times 10^3\ M_\odot\ \mathrm{pc}^{-2}$, whereas we find a value of $\sim 1.4 \times 10^3\ M_\odot\ \mathrm{pc}^{-2}$ for the surrounding medium; hence, we find a difference of a factor of ∼3. This value would increase even more when taking the surface density of the CO 1−0 (500−1000 $M_\odot\ \mathrm{pc}^{-2}$, Aalto & Hüttemeister 2000) into account instead. The difference between the obtained values from our CO 2−1 observations and the CO 1−0 data from Aalto & Hüttemeister (2000) is that we do suffer from resolving out large parts of the lower brightness gas due to the high resolution of these observations.

The bulk of the star formation ongoing in the SSCs that are distributed on extended scales is not associated with the regions of highest surface brightness density (Figs. 8, 9). The clusters identified with the highest Hα SFR, however, are located in this high surface density region (Hancock et al. 2006). Using the CO 2−1 surface brightness density, the Kennicutt-Schmidt law predicts an SFR of ∼4.9 $M_\odot\ \mathrm{yr}^{-1}$, which within the error bars is in good agreement with the 6−7 $M_\odot\ \mathrm{yr}^{-1}$ value that Aalto & Hüttemeister (2000) estimated from the FIR but is much below the value of ∼46 $M_\odot\ \mathrm{yr}^{-1}$ that Hancock et al. (2006) derive from their Hα observations. The SFE we obtained from the highest surface brightness density CO 2−1 emission is $\sim 1.5 \times 10^{-8}\ \mathrm{yr}^{-1}$. Although NGC 4194 has a brightness surface density of one magnitude lower than typical ULIRGs, its SFEs rival that of these extraordinary objects (e.g., SFE(Arp 220) $\sim 2 \times 10^{-8}$, Franceschini 2003). Compared to values in typical mergers, the star formation in NGC 4194 is two orders of magnitude more efficient (Rownd & Young 1999).

Although the gas surface density at the center of NGC 4194 has now increased to $\sim 4.1 \times 10^3\ M_\odot\ \mathrm{pc}^{-2}$, these values show that the surface density even in the densest regions in the center is still lower by one order of magnitude compared to the gas in the centers of ULIRGs like Arp 220 or Mrk 231 that have

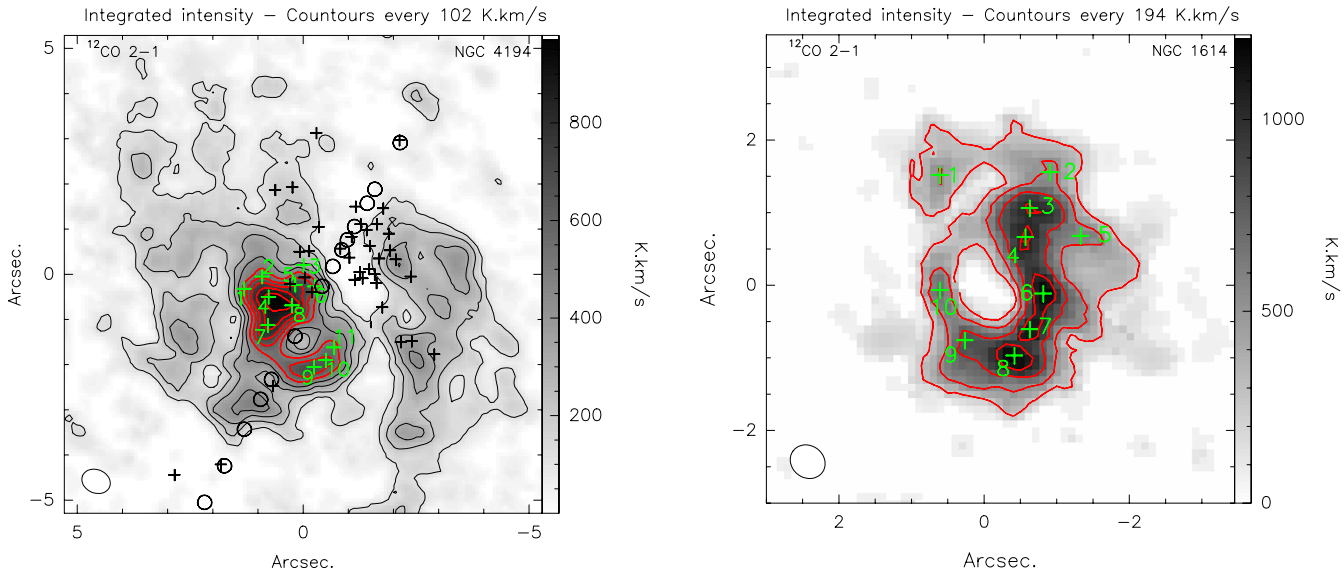

Fig. 9. Comparison of the nuclear molecular rings of NGC 4194 (*left*) and NGC 1614 (*right*, König et al. 2013). The images are scaled to represent a field of view of ∼2000 pc. Contours emphasized in red represent the CO 2−1 ring structures in the Medusa (1″ ∼ 189 pc) and NGC 1614 (1″ ∼ 310 pc); green crosses mark the positions of the GMAs in the Medusa and NGC 1614. Black crosses represent the UV-identified star clusters (Weistrop et al. 2004), and black circles indicate the star clusters identified in visible light in a 0.5″ wide slit (Hancock et al. 2006) in the Medusa.

surface densities of up to $\sim 3.3 \times 10^4\ M_\odot\ \mathrm{pc}^{-2}$ (Bryant & Scoville 1999). The central high surface brightness gas density values in NGC 4194 are comparable to numbers for other similar sources, such as NGC 1614 ($\sim 3.1 \times 10^3\ M_\odot\ \mathrm{pc}^{-2}$, König et al. 2013) and NGC 5218 ($\sim 1.8 \times 10^3\ M_\odot\ \mathrm{pc}^{-2}$, Cullen et al. 2007).

4.4. Infalling gas

1.4 GHz radio continuum observations show two compact radio components at the center of NGC 4194 (Beswick et al. 2005). They concluded that there is the possibility of a weak, buried AGN that contributes to the powering of the star formation. The position that is inferred from the radio continuum brightness peak coincides with the velocity dispersion peak, which we find in our CO 2−1 data (Fig. 2a). The rotation curve fitted to the CO 2−1 data cube (Fig. 2a, Sect. 3.1.2) further indicated the location of the dynamical center just ∼0.4″ toward the south of the radio continuum and the velocity dispersion peaks. This is in positional agreement within one beam size.

It is possible that the nucleus is fed by molecular gas returning via the dust lane. Bournaud et al. (2005) have shown that the gas in minor mergers that is brought in by a disturbing galaxy companion is generally found at large radii in the merger remnant. Gas located in this largest scale gas reservoir is then returned to the system via tidal tails, where it often ends up forming rings, which might be associated with or appear as dust lanes seen edge-on. In NGC 4194, a number of dust lanes has been found. The dust lanes most probably playing a role in the feeding of the AGN are the two large dust lanes to the east of the nucleus and a smaller one just northeast of the AGN. All those dust lanes are associated with the CO emission (Aalto & Hüttemeister 2000, see also Fig. 1b) and might funnel the CO from the larger scale molecular gas reservoir, as traced by the CO 1−0 emission, to the center and ultimately to the AGN. We found evidence for this scenario for example in the western part of the molecular gas distribution in the velocity field (Figs. 1c, d) and the map showing the residuals from the subtraction of the rotation curve (Fig. 2b), which show typical features of streaming motions as, for example, found in M 51 (Aalto et al. 1999) and M 83 (Rand et al. 1999).

Another mode of transport providing gas to the center of NGC 4194 might be streaming motions. We found indications for streaming motions in the western arm of NGC 4194. Gas could be piled up in the center of the galaxy due to orbit crowding processes of inflowing gas streams. In the galactic potential, the gas brought in through the streams encounters shocks and migrates to new orbits accumulating in these locations.

5. Comparisons to other galaxies

Comparisons between the features of NGC 4194 and other interacting galaxies with similar types of structure can help in the interpretation of our data. In this section, we consider how the properties of NGC 4194 relate to those observed in a comparison sample of interacting galaxies and galaxies with shells/bubbles.

5.1. Comparison to other minor axis dust lane minor mergers

One galaxy sharing a number of properties with NGC 4194 is the S+s minor merger NGC 1614. Both galaxies are associated with large reservoirs of molecular gas (e.g., Aalto & Hüttemeister 2000; Olsson et al. 2010; König et al. 2013). Whereas the star formation in NGC 1614 is mostly associated with molecular gas (CO) and other tracers like Paα, radio continuum, etc. (König et al. 2013), most of the star formation in NGC 4194 is taking place in star clusters (Weistrop et al. 2004; Hancock et al. 2006), which are not associated with the bulk of the ^{12}CO emission, but instead, mostly with lower surface brightness gas to the west of the mergers nucleus.

Looking into the molecular gas content in these two galaxies in more detail, NGC 4194 and NGC 1614 share even more properties. In both galaxies, a large reservoir of CO 1−0 emission is associated with the minor axis dust lanes crossing the mergers main body. This association between molecular gas and dust lanes led to suggestions that the dust lanes are playing a key role in the transport of the molecular gas into the centers of

Table 2. Overview of the parameters of galaxies compared to NGC 4194.

Galaxy	Merger/	Presence of			Ring key properties		Shell key properties			Reference
	interaction	a bar	a ring	a shell	radius [pc]	mass [$M_\odot$]	radius [pc]	v_{exp}[a] [km s^{-1}]	mass [$M_\odot$]	
NGC 4194	+	+	+	+	320	4.4×10^8	180	55	2.3×10^8	1), 2), 3)
NGC 1614	+	(+)[b]	+	–	500	8.3×10^8	–	–	–	4)
NGC 5218	+[c]	+	+	+	470	7×10^8	150	30	7×10^7	5), 6)
NGC 3718	+[c]	+	–	–	–	–	–	–	–	7), 8)
NGC 4441	+	–	(+)[b]	+	875	4.1×10^8	[d]	[d]	[d]	9), 10)
M 82	+[e]	+	+	+	200	3×10^7	65[e]	45[e]	8×10^6[e]	11), 12)
NGC 253	–	+	–	+	–	–	130	50	$\sim10^6$	13)

Notes. [(a)] Expansion velocity. [(b)] Its presence is still under discussion. [(c)] Part of an interacting galaxy pair: NGC 5218 ⇄ NGC 5216, NGC 3718 ⇄ NGC 3729, M 82 ⇄ M 81. [(d)] No values given in the literature for the optical shells. [(e)] Values are for the molecular superbubble.

References. 1) This work; 2) Beck et al. (2014); 3) Jütte et al. (in prep.); 4) König et al. (2013); 5) Olsson et al. (2007); 6) Gallagher & Parker (2010); 7) Sparke et al. (2009); 8) Krips et al. (2005); 9) Manthey et al. (2008); 10) Jütte et al. (2010); 11) Weiß et al. (1999); 12) Nakai et al. (1987); 13) Sakamoto et al. (2006).

galaxies of this type (minor mergers). Both galaxy centers harbor ring-like molecular structures that are clearly identified in high-resolution ^{12}CO 2–1 observations (König et al. 2013, this work) that might be connected to the larger scale CO 1–0 reservoirs via the respective dust lanes. The ring-structures are, however, different in size and mass. The ring in NGC 1614 is twice as large and twice as massive (König et al. 2013) than the shell complex in NGC 4194 (Fig. 9, Table 2). Both ring-like structures are located off the actual nuclei of their galaxies: the ring in NGC 1614 is located symmetrically off-nucleus with its center located right at the galaxy's nucleus (König et al. 2013), whereas the high density gas complex in NGC 4194 including the shell is located asymmetrically off nucleus. Only the gas to the north of the shell, containing the AGN, is located at the very nucleus of this galaxy. Both rings are closely associated with radio continuum emission, whereas the emission in NGC 1614 is actually associated with the ring, the radio continuum in NGC 4194 has a secondary peak at the center of the shell but does not coincide with most of the CO emission located in the shell. It does seem as if the radio continuum in NGC 4194 is avoiding the regions filled with CO in the shell. Furthermore, we have identified GMAs (Fig. 9) in both NGC 4194 and NGC 1614–11 in NGC 4194 and ten in NGC 1614. The GMAs in both minor mergers are associated with the dust lanes. In general, the GMAs in NGC 4194 are smaller in size and mass then the ones in NGC 1614. This is most probably due to the AGN-shell-complex in NGC 4194 itself being much smaller than the ring in NGC 1614.

Other nearby minor axis dust lane galaxies at different evolutionary stages in the merger sequence share some of these properties as well (e.g., NGC 5218, NGC 3718, and NGC 4441). The object NGC 5218 is a merger at an earlier evolutionary stage with a molecular ring about 2.5 times larger and twice more massive than the ring in NGC 4194 (Table 2 Cullen et al. 2007; Olsson et al. 2007). Two galaxies at a later evolutionary stage in the merger sequence are NGC 3718 and NGC 4441. In their morphology, NGC 3718 and NGC 4441 are very similar to NGC 4194; they have tidal tails and minor axis dust lanes crossing the galaxies. Closely associated with these features are molecular gas reservoirs extended out to large scales (e.g., Pott et al. 2004; Krips et al. 2005; Jütte et al. 2010) as in NGC 4194. Like NGC 4194, NGC 3718 hosts a large number of star clusters (Trinh et al. 2006). Both mergers also harbor molecular disks/ring-like structures at their centers (Schwarz 1985; Pott et al. 2004; Krips et al. 2005; Sparke et al. 2009; Jütte et al. 2010).

In a nutshell, galaxies with minor axis dust lanes involved in interactions/mergers can show extended molecular gas emission over scales of several kpc, and many harbor molecular gas rings at their centers. There is no obvious correlation between the size and mass of the observed molecular rings with the stage of the interaction/merger process the comparison galaxies represent.

5.2. Shells in other galaxies

A number of shells and bubbles have been discovered in external galaxies using different atomic and molecular gas tracers (e.g., HI, OH, CO, Weiß et al. 1999; Wills et al. 2002; Sakamoto et al. 2006; Olsson et al. 2007; Argo et al. 2010). Nearby starburst galaxies known to host molecular shells/bubbles are M 82, NGC 253, and NGC 5218. These bubble hosts are no mergers, but M 82 and NGC 5218 are involved in interactions. All three of them have a bar transporting molecular gas to the galaxies center (Petitpas & Wilson 2000; Mauersberger et al. 1996; Olsson et al. 2007) like NGC 4194 (Beck et al. 2014; Jütte et al., in prep.).

One process, that causes the formation of shells/bubbles can be the explosion of a large number of supernovae, as suggested for the bubbles in M 82 (e.g., Wills et al. 2002; Argo et al. 2010) and the shell in NGC 5218 (Olsson et al. 2007). It has been determined that the energy output of up to several thousand type II supernovae is necessary to reach the current extents that are found for these structures. An alternative scenario for shell/bubble formation is that they might be caused by stellar winds coming from massive SSCs, as suggested for the bubbles in NGC 253 (Sakamoto et al. 2006). NGC 4194 does have a large population of star clusters, but the majority of these clusters is located away from the bulk of the molecular gas. In particular, we do not find a large conglomerate of star clusters at the center of the molecular shell in NGC 4194. This points toward supernova explosions as the driving mechanism of the shell in this galaxy.

An in-detail comparison between the shells/bubbles in these three galaxies with the shell in NGC 4194 (for more details see Table 2) shows that the shell in NGC 4194 is older, has a larger size, expands with a higher velocity, and is more massive than the shells/bubbles found in the starburst galaxies M 82, NGC 253, and NGC 5218.

This shows that NGC 4194 shares properties with several of the comparison galaxies – for example, being a merger, having dust lanes, harboring shells/bubbles and/or GMAs, having asymmetric molecular ring-like structures, and massive star

clusters. However, we always found significant differences as well. Therefore, NGC 4194 cannot be classified as a typical barred spiral galaxy, or a typical merger of any flavor; it remains a very interesting yet puzzling object.

6. Summary

We studied the properties of the molecular gas in the center of NGC 4194 using high angular resolution ^{12}CO 2−1 emission line observations.

1. We found a ring-like structure, the Eye of the Medusa, at the center of NGC 4194. A large part of the gas in this region of high surface brightness is associated with the major dust lane. The structure contains molecular gas associated with the AGN and a molecular shell located southeast of the nucleus.
2. The event causing the formation of the molecular shell southeast of the dynamical center of NGC 4194 was most probably a number of supernovae explosions, which now pushes the molecular gas outward.
3. The kinematics of the molecular gas distribution suggest that gas is transported along the dust lanes to the center of NGC 4194, where it replenishes the gas in the Eye. Smaller dust lanes in the very center, together with the pressure provided by the expanding material in the shell, then funnel this gas to the immediate surroundings of the AGN.
4. We identified individual GMAs in the Eye, which are associated with both the shell structure and the gas surrounding the AGN. The GMAs are not associated with star clusters previously identified in the UV and visible wavelength regimes.

In summary, we found that NGC 4194 is a very interesting lab to study different physical properties of the molecular gas in different states. It is remarkable how well-ordered the velocity field looks when comparing all the different processes going on at different scales of this merger. We believe we found another example of a minor merger, besides NGC 1614, where molecular gas is transported via the dust lanes to the very center of the galaxy. There, we found molecular gas associated with the AGN at the dynamical center and with a shell to the southeast of the very nucleus, which is most likely formed by explosions of supernovae. The GMAs we located in the central molecular structure might be the result of the formation of denser gas resulting from shocks from the supernovae explosions.

In spite of these results, many questions remain to be answered, such as the origin of the gas surrounding the AGN, the feeding of the AGN itself on even smaller scales, and the origin of the GMAs, or how the kinematics of cold molecular gas affect the evolution of star formation and nuclear activity in minor mergers in general. A more detailed study of the molecular gas content of NGC 4194 on different spatial scales is needed to address these questions. New studies with instruments, such as the PdBI and the SMA, will enable us to answer them.

Acknowledgements. We thank the referee for useful comments. S.A. thanks the Swedish Research Council (grant 621-2011-414) and the Swedish National Space Board (SNSB, grant 145/11:1-3) for support. J.S.G. thanks the College of Letters & Science, University of Wisconsin-Madison for partial support of this work. The Submillimeter Array is a joint project between the Smithsonian Astrophysical Observatory and the Academia Sinica Institute of Astronomy and Astrophysics and is funded by the Smithsonian Institution and the Academia Sinica. MERLIN/eMERLIN is a National Facility operated by the University of Manchester at Jodrell Bank Observatory on behalf of STFC. AIPS is produced and maintained by the National Radio Astronomy Observatory, a facility of the National Science Foundation operated under cooperative agreement by Associated Universities, Inc. This research has made use of the NASA/IPAC Extragalactic Database (NED) which is operated by the Jet Propulsion Laboratory, California Institute of Technology, under contract with the National Aeronautics and Space Administration.

References

Aalto, S., & Hüttemeister, S. 2000, A&A, 362, 42
Aalto, S., Hüttemeister, S., Scoville, N. Z., & Thaddeus, P. 1999, ApJ, 522, 165
Aalto, S., Hüttemeister, S., & Polatidis, A. G. 2001, A&A, 372, L29
Aalto, S., Beswick, R., & Jütte, E. 2010, A&A, 522, A59
Argo, M. K., Pedlar, A., Beswick, R. J., Muxlow, T. W. B., & Fenech, D. M. 2010, MNRAS, 402, 2703
Armus, L., Heckman, T. M., & Miley, G. K. 1990, ApJ, 364, 471
Beck, S. C., Lacy, J., Turner, J., Greathouse, T., & Neff, S. 2014, ApJ, 787, 85
Bernard-Salas, J., Spoon, H. W. W., Charmandaris, V., et al. 2009, ApJS, 184, 230
Beswick, R. J., Aalto, S., Pedlar, A., & Hüttemeister, S. 2005, A&A, 444, 791
Bournaud, F., Jog, C. J., & Combes, F. 2005, A&A, 437, 69
Brandt, J. C. 1960, ApJ, 131, 293
Bryant, P. M., & Scoville, N. Z. 1999, AJ, 117, 2632
Casoli, F., Dupraz, C., & Combes, F. 1992, A&A, 264, 55
Chevalier, R. A. 1974, ApJ, 188, 501
Clark, B. G. 1980, A&A, 89, 377
Combes, F. 1988, in NATO ASIC Proc. 232: Galactic and Extragalactic Star Formation, eds. R. E. Pudritz, & M. Fich, 475
Condon, J. J., Helou, G., Sanders, D. B., & Soifer, B. T. 1990, ApJS, 73, 359
Cullen, H., Alexander, P., Green, D. A., & Sheth, K. 2007, MNRAS, 376, 98
de Grijs, R., Anders, P., Bastian, N., et al. 2003, MNRAS, 343, 1285
Franceschini, A. 2003, in Galaxies at High Redshift, eds. I. Pérez-Fournon, M. Balcells, F. Moreno-Insertis, & F. Sánchez, 69
Gallagher, III, J. S., & Parker, A. 2010, ApJ, 722, 1962
Hancock, M., Weistrop, D., Nelson, C. H., & Kaiser, M. E. 2006, AJ, 131, 282
Hsieh, P.-Y., Matsushita, S., Liu, G., et al. 2011, ApJ, 736, 129
Jütte, E., Aalto, S., & Hüttemeister, S. 2010, A&A, 509, A19
Kaaret, P., & Alonso-Herrero, A. 2008, ApJ, 682, 1020
Kennicutt, R. C., & Evans, N. J. 2012, ARA&A, 50, 531
König, S., Aalto, S., Muller, S., Beswick, R. J., & Gallagher, J. S. 2013, A&A, 553, A72
Krips, M., Eckart, A., Neri, R., et al. 2005, A&A, 442, 479
Larsen, S. S. 2002, AJ, 124, 1393
Larson, R. B. 1981, MNRAS, 194, 809
Lehmer, B. D., Alexander, D. M., Bauer, F. E., et al. 2010, ApJ, 724, 559
Lindroos, L. 2011, Masters thesis, Chalmers University of Technology
Manthey, E., Hüttemeister, S., Aalto, S., Horellou, C., & Bjerkeli, P. 2008, A&A, 490, 975
Mauersberger, R., Henkel, C., Wielebinski, R., Wiklind, T., & Reuter, H.-P. 1996, A&A, 305, 421
Mora, M. D., Larsen, S. S., Kissler-Patig, M., Brodie, J. P., & Richtler, T. 2009, A&A, 501, 949
Nakai, N., Hayashi, M., Handa, T., et al. 1987, PASJ, 39, 685
Narayanan, D., Krumholz, M. R., Ostriker, E. C., & Hernquist, L. 2012, MNRAS, 421, 3127
Olsson, E., Aalto, S., Thomasson, M., Beswick, R., & Hüttemeister, S. 2007, A&A, 473, 389
Olsson, E., Aalto, S., Thomasson, M., & Beswick, R. 2010, A&A, 513, A11
Petitpas, G. R., & Wilson, C. D. 2000, ApJ, 538, L117
Pott, J.-U., Hartwich, M., Eckart, A., et al. 2004, A&A, 415, 27
Rand, R. J., Lord, S. D., & Higdon, J. L. 1999, ApJ, 513, 720
Rownd, B. K., & Young, J. S. 1999, AJ, 118, 670
Sakamoto, K., Ho, P. T. P., Iono, D., et al. 2006, ApJ, 636, 685
Sakamoto, K., Ho, P. T. P., Mao, R.-Q., Matsushita, S., & Peck, A. B. 2007, ApJ, 654, 782
Sandstrom, K. M., Leroy, A. K., Walter, F., et al. 2013, ApJ, 777, 5
Schwarz, U. J. 1985, A&A, 142, 273
Shlosman, I., Frank, J., & Begelman, M. C. 1989, Nature, 338, 45
Solomon, P. M., Rivolo, A. R., Barrett, J., & Yahil, A. 1987, ApJ, 319, 730
Sparke, L. S., van Moorsel, G., Schwarz, U. J., & Vogelaar, M. 2009, AJ, 137, 3976
Trinh, C. Q., Sparke, L. S., & Gallagher, J. S. 2006, BAAS, 38, 924
van der Laan, T. P. R., Schinnerer, E., Emsellem, E., et al. 2013, A&A, 556, A98
Vogel, S. N., Kulkarni, S. R., & Scoville, N. Z. 1988, Nature, 334, 402
Weiß, A., Walter, F., Neininger, N., & Klein, U. 1999, A&A, 345, L23
Weistrop, D., Eggers, D., Hancock, M., et al. 2004, AJ, 127, 1360
Weistrop, D., Nelson, C. H., Angione, R., et al. 2012, AJ, 143, 98
Wills, K. A., Pedlar, A., & Muxlow, T. W. B. 2002, MNRAS, 331, 313